

Combined analysis of the reactions $pp \rightarrow pp, \pi d \rightarrow \pi d$, and $\pi d \rightarrow pp$

Chang Heon Oh, Richard A. Arndt, Igor I. Strakovsky,* and Ron L. Workman
 Department of Physics, Virginia Polytechnic Institute and State University, Blacksburg, Virginia 24061
 (Received 3 February 1997)

Results are presented for a combined analysis of the reactions $pp \rightarrow pp, \pi d \rightarrow \pi d$, and $\pi d \rightarrow pp$ over the \sqrt{s} interval from the pion threshold to approximately 2.4 GeV. These results for $\pi d \rightarrow pp$ and πd elastic scattering are superior to our previous analyses of these reactions. In particular, the overall phase in $\pi d \rightarrow pp$ has now been determined. Comparisons are made with previous (separate and combined) analyses of this two-nucleon system. [S0556-2813(97)03508-5]

PACS number(s): 11.80.Et, 13.75.Cs, 25.40.Ep, 25.80.Hp

I. INTRODUCTION

An understanding of the NN interaction is fundamental to studies of the more general πNN problem [1]. Below 1 GeV, in proton laboratory kinetic energy T_p for the NN system, the dominant channels contributing to NN inelasticity are πd and $N\Delta$ [2]. At these energies, it is useful to employ a multichannel formalism in analyzing all existing data simultaneously. In the present work, we have used the K -matrix formalism in order to unify the analysis of several reactions ($pp \rightarrow pp$ [3], $\pi d \rightarrow \pi d$ [5], and $\pi d \rightarrow pp$ [7]) which we have, in the past, considered separately. The range of \sqrt{s} was chosen to include all of our results for the pion-induced reactions ($T_\pi = 0 - 500$ MeV).

Clearly, we are not the first to consider this problem. A joint analysis of these three reactions, in a narrow energy range near the $N\Delta$ threshold, was recently reported by Nagata *et al.* [8]. This work used a mix of model-based and phenomenological results to investigate possible narrow structures in these reactions. An older work by Edwards [9] used the multichannel K -matrix formalism to study the $J^P = 2^+$ and 3^- states associated with dibaryon candidates.

The present analysis differs from those carried out previously in a number of important respects. We did not restrict our study to partial waves containing interesting structures. For pp elastic scattering, all waves with $J \leq 7$ were used. Partial waves with $J \leq 5$ were retained for both πd elastic scattering and $\pi d \rightarrow pp$. In addition, the K -matrix parameters were determined solely from our fits to the available databases for each separate reaction. No results of outside analyses or any model approaches were used as constraints. As a result, the amplitudes found in our K -matrix fits are as “unbiased” as those coming from the separate analyses [4].

In Sec. II, we will outline the K -matrix formalism used in this analysis. The combined and separate analyses will be compared in Sec. III. Conclusions and suggestions for further study will be given in Sec. IV.

II. FORMALISM

In order to analyze the reaction $\pi d \rightarrow pp$ along with elastic pp and πd scattering, we have constructed a K -matrix formalism having $pp, \pi d$, and $N\Delta$ channels. The energy dependence of our global fit was obtained through a coupled-channel K -matrix form in order to ensure that unitarity would not be violated. The “ $N\Delta$ ” channel is added to account for all channels other than pp and πd . The most important thresholds are illustrated schematically in Fig. 1. That this catchall channel is indeed mainly $N\Delta$ can be seen in Fig. 2, where the total cross sections for pp and πd scattering are broken into their components.

As the elastic pp partial-wave analysis is far superior to the πd elastic and $\pi d \rightarrow pp$ analyses, we have carried out fits in which the pp partial waves were held fixed. (The partial-wave decomposition of the $pp, \pi d$, and $N\Delta$ systems is given in Table I.) As described below, the pp amplitudes were used to fix some elements of the K matrix, while the others were determined from a fit to the combined πd elastic and $\pi d \rightarrow pp$ databases.

States of a given total angular momentum and parity (J^P) were parametrized by a 4×4 K matrix (K_J) which coupled to an appropriate $N\Delta$ channel. Spin-mixed (2×2) pp states couple to unmixed πd states, and unmixed pp states couple to spin-mixed (2×2) πd states; so the πd - pp system is always represented by a 3×3 matrix. For

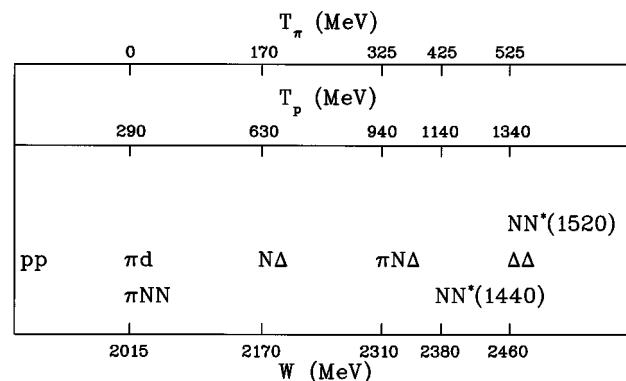


FIG. 1. Energy scale in terms of the total center-of-mass energy (\sqrt{s}) and the incident kinetic energies of the $pp(T_p)$ and $\pi d(T_\pi)$ initial states. The locations of relevant thresholds are also displayed.

*On leave from St. Petersburg Nuclear Physics Institute, Gatchina, St. Petersburg, 188350 Russia.

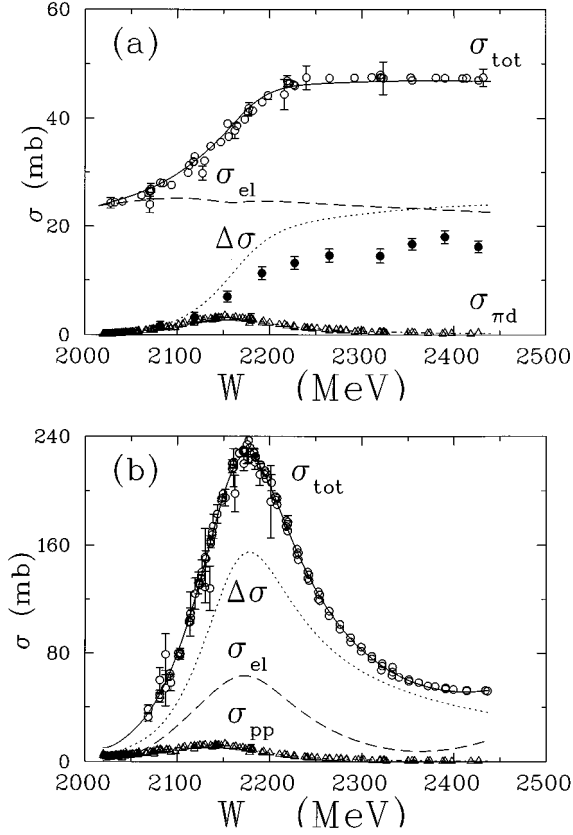


FIG. 2. (a) Total pp cross sections σ_{tot} (solid line) and total elastic cross sections σ_{el} (dashed line) correspond to the C500 solution. Data for σ_{tot} (open circles) are taken from the SAID database [4]. Dash-dotted lines, corresponding to the C500 solution, show the total cross sections ($\sigma_{\pi d}$) for $pp \rightarrow \pi d$. The corresponding data from the SAID database [4] are plotted as open triangles. The remainder ($\Delta\sigma$) is given by $\sigma_{\text{tot}} - \sigma_{\text{el}} - \sigma_{\pi d}$ and plotted as a dotted line. Total cross sections for the reactions $pp \rightarrow \Delta^+ p + \Delta^+ n$ [2] are plotted as dark circles. (b) Total πd cross sections σ_{tot} (solid line) and total elastic cross sections σ_{el} (dashed line) correspond to the C500 solution. Data for σ_{tot} (open circles) are taken from the SAID database [4]. Dash-dotted lines (C500) show the total cross sections (σ_{pp}) for $\pi d \rightarrow pp$. The corresponding data from the SAID database [4] are plotted as open triangles. The remainder ($\Delta\sigma$) is given by $\sigma_{\text{tot}} - \sigma_{\text{el}} - \sigma_{pp}$ and plotted as a dotted line.

example, the T matrix (T_J) for $J^P = 2^+$ (unmixed pp states) is given by

$$T_2 = \begin{pmatrix} pp & \pi d_- & \pi d_+ \\ {}^1D_2 & {}^1D_2P & {}^1D_2F \\ {}^1D_2P & {}^3P_2 & \epsilon_2 \\ {}^1D_2F & \epsilon_2 & {}^3F_2 \end{pmatrix} \begin{pmatrix} pp \\ \pi d_- \\ \pi d_+ \end{pmatrix}, \quad (1)$$

whereas the T matrix for $J^P = 2^-$ (mixed pp states) is

$$T_2 = \begin{pmatrix} pp_- & pp_+ & \pi d \\ {}^3P_2 & \epsilon_2 & {}^3P_2D \\ \epsilon_2 & {}^3F_2 & {}^3F_2D \\ {}^3P_2D & {}^3F_2D & {}^3D_2 \end{pmatrix} \begin{pmatrix} pp_- \\ pp_+ \\ \pi p \end{pmatrix}. \quad (2)$$

TABLE I. Partial-wave decomposition of pp , πd , and $N\Delta$ systems.

J^P	πd	pp	$N\Delta$
0^+	3P_0	1S_0	5D_0
0^-		3P_0	3P_0
1^+	3P_1 3P_1		${}^3S_1, {}^3D_1$ 5D_1
1^-	${}^3S_1, {}^3D_1$ ${}^3S_1, {}^3D_1$	3P_1 3P_1	3P_1 ${}^5P_1, {}^5F_1$
2^+	${}^3P_2, {}^3F_2$ ${}^3P_2, {}^3F_2$ ${}^3P_2, {}^3F_2$	1D_2 1D_2 1D_2	3D_2 ${}^5S_2, {}^5D_2$ ${}^5D_2, {}^5G_2$
2^-	3D_2 3D_2	${}^3P_2, {}^3F_2$ ${}^3P_2, {}^3F_2$	${}^3P_2, {}^3F_2$ ${}^5P_2, {}^5F_2$
3^+	3F_3 3F_3		${}^3D_3, {}^3G_3$ ${}^5D_3, {}^5G_3$
3^-	${}^3D_3, {}^3G_3$ ${}^3D_3, {}^3G_3$ ${}^3D_3, {}^3G_3$	3F_3 3F_3 3F_3	${}^3P_3, {}^3F_3$ ${}^5P_3, {}^5F_3$ ${}^5F_3, {}^5H_3$
4^+	${}^3F_4, {}^3H_4$ ${}^3F_4, {}^3H_4$ ${}^3F_4, {}^3H_4$	1G_4 1G_4 1G_4	3G_4 ${}^5D_4, {}^5G_4$ ${}^5G_4, {}^5I_4$
4^-	3G_4 3G_4	${}^3F_4, {}^3H_4$ ${}^3F_4, {}^3H_4$	${}^3F_4, {}^3H_4$ ${}^5F_4, {}^5H_4$

The subscripts \pm denote states with $L = J \pm 1$. In the above, the mixing parameters (ϵ) for elastic pp and πd scattering are different. For the reaction $\pi d \rightarrow pp$, the notation (${}^{2S_{pp}+1}L_J^{pp}L\pi$) of Ref. [7] is used.

Adding an $N\Delta$ channel results in a 4×4 T matrix. Dropping the J subscript, we write the K matrix as

$$K = \begin{pmatrix} K_{pp} & K_0 \\ \bar{K}_0 & K_i \end{pmatrix}, \quad (3)$$

TABLE II. Comparison of the combined analysis (C500) and our previous (separate) analyses. WI96 for $pp \rightarrow pp$ [3], SM94 for $\pi d \rightarrow \pi d$ [5], and SP96 for $\pi d \rightarrow pp$ [7]. The relevant energy ranges are: $T_\pi = 0-500$ MeV, $T_p = 288-1290$ MeV, and $\sqrt{s} = 2015-2440$ MeV.

Reaction	Separate χ^2/data	Combined χ^2/data
$pp \rightarrow pp$	17380/10496	17380/10496
$\pi d \rightarrow \pi d$	2745/1362	2418/1362
$\pi d \rightarrow pp$	7716/4787	7570/4787

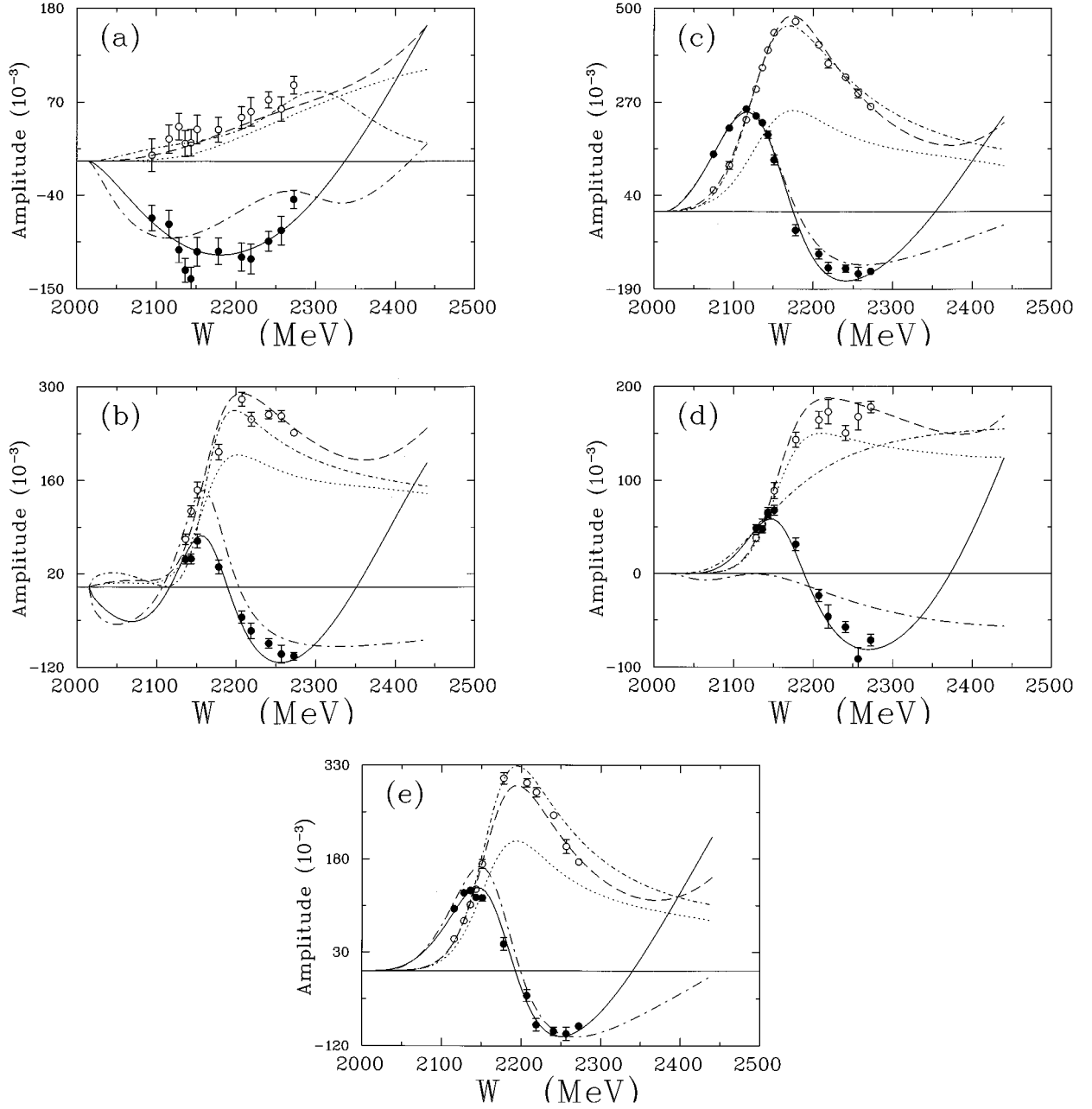


FIG. 3. Partial-wave amplitudes of the reaction $\pi d \rightarrow \pi d$ from $T_\pi = 0$ to 500 MeV. Solid (dashed) curves give the real (imaginary) parts of amplitudes corresponding to the C500 solution. Our previous analysis (SM94) [5] is plotted with long dash-dotted (real part) and short dash-dotted (imaginary part) lines. The dotted curve gives the value of $\text{Im } T - T^2 - T_{\text{sf}}^2$, where T_{sf} is the spin-flip amplitude for C500. The real (imaginary) parts of single-energy solutions are plotted as solid (open) circles. All amplitudes have been multiplied by a factor of 10^3 and are dimensionless. Plotted are the dominant partial-wave amplitudes: (a) ${}^3P_0(0^+)$, (b) ${}^3S_1(1^-)$, (c) ${}^3P_2(2^+)$, (d) ${}^3D_2(2^-)$, and (e) ${}^3D_3(3^-)$.

where K_{pp} is the elastic pp scattering submatrix, K_0 and \bar{K}_0 are row and column vectors, and K_i is the submatrix of channels involving πd and $N\Delta$ states. This K matrix can be reexpressed as a T matrix

$$T = \begin{pmatrix} T_{pp} & T_0 \\ \bar{T}_0 & T_i \end{pmatrix} \quad (4)$$

using the relation $T = K(1 - iK)^{-1}$. We then have the correspondence [10]

$$T_{pp} = \bar{K}_{pp}(1 - i\bar{K}_{pp})^{-1}, \quad (5)$$

where

$$\bar{K}_{pp} = K_{pp} + iK_0(1 - iK_i)^{-1}\bar{K}_0. \quad (6)$$

In order to ensure an exact fit to the pp elastic T matrix, given by our most recent analysis of NN elastic scattering to 1.6 GeV [3], we take

$$K_{pp} = T_{pp}(1 + iT_{pp}) - iK_0(1 - iK_i)^{-1}\bar{K}_0. \quad (7)$$

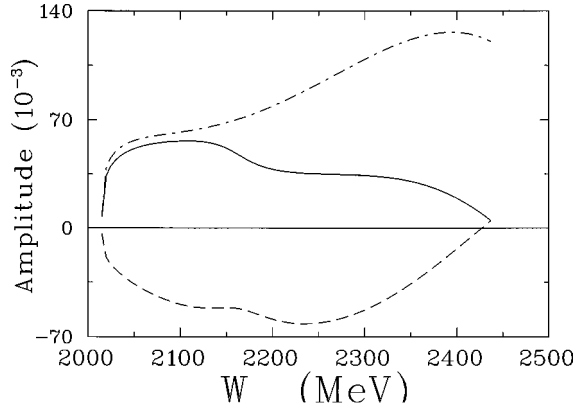


FIG. 4. Comparison of the 3P_1S partial waves for $\pi d \rightarrow pp$ obtained in the separate and combined fits. The real (imaginary) part of solution C500 is plotted as a solid (dashed) line. The purely real partial wave from our separate analysis (SP96) [7] is plotted as a dot-dashed line.

The matrix elements are then expanded as polynomials in the pion energy times appropriate phase-space factors. The πd elastic and $\pi d \rightarrow pp$ T -matrix elements are extracted from T_0 and T_i .

III. PARTIAL-WAVE AMPLITUDES

We have fitted the amplitudes for $pp \rightarrow pp$ and the existing databases for $\pi d \rightarrow pp$, and $\pi d \rightarrow \pi d$, using the K -matrix formalism outlined in Sec. II. (Detailed relations between the amplitudes and observables are given in our previous publications [11].) The πd elastic and $\pi d \rightarrow \pi d$ databases used in this analysis are described in Refs. [5] and [7], and are available from the authors [4]. The overall χ^2 for our combined analysis is actually superior to that found in our single-reaction analyses. This is due to the improved parametrization scheme. A comparison is given in Table II. We should emphasize that the amplitudes for pp elastic scattering are the same as those given in Ref. [3]. As mentioned

TABLE III. Comparison of single-energy (binned) and energy-dependent combined analyses of πd elastic scattering data. N_{prm} is the number of parameters varied in the single-energy fits. χ_E^2 is due to the energy-dependent fit (C500) taken over the same energy interval.

T_π (MeV)	Range (MeV)	N_{prm}	χ^2/data	χ_E^2
65	58.0–72.0	2	106/54	102
87	72.0–92.0	6	20/24	21
111	107.5–125.2	10	68/82	66
125	115.0–134.0	12	155/170	184
134	124.0–142.8	14	315/258	344
142	133.0–152.0	16	356/284	397
151	141.0–160.6	16	193/154	216
182	174.0–189.5	18	302/168	396
216	206.0–220.0	18	158/99	200
230	220.0–238.0	18	64/53	111
256	254.0–260.0	16	132/125	185
275	270.5–284.4	16	22/40	42
294	284.4–300.0	16	267/132	324

TABLE IV. Comparison of single-energy (binned) and energy-dependent combined analyses of $\pi d \rightarrow pp$ reaction data. N_{prm} is the number of parameters varied in the single-energy fits. χ_E^2 is due to the energy-dependent fit (C500) taken over the same energy interval.

T_π (MeV)	Range (MeV)	N_{prm}	χ^2/data	χ_E^2
25	12.8–37.4	10	527/241	542
50	37.6–60.7	12	188/168	205
75	62.9–87.3	14	590/426	628
100	91.0–114.0	14	1263/611	1379
125	113.8–137.1	16	729/512	756
150	140.0–162.0	20	743/630	792
175	165.0–187.3	22	343/280	426
200	191.3–210.3	20	120/193	153
225	217.9–235.9	22	217/229	291
250	238.9–262.0	22	595/483	685
275	264.9–285.1	22	204/109	280
300	291.6–307.4	24	198/212	235
325	318.9–330.0	24	142/161	234
350	341.4–360.3	24	201/185	233
375	371.4–375.7	24	32/26	42
400	390.0–400.0	24	19/28	34
425	417.0–420.0	24	50/28	55
450	437.6–456.5	22	122/48	231
475	473.8–487.4	22	24/24	39
500	495.9–506.5	22	49/45	281

above, this feature was built into our K -matrix parametrization. For this reason, we have omitted plots of the pp amplitudes [4].

The results for πd elastic scattering are also qualitatively similar, up to the limit of our single-energy analyses. In Fig. 3 we compare the main partial waves from our single-reaction analysis [5] and combined analysis (solution C500). Significant differences begin to appear above a pion laboratory kinetic energy of 300 MeV or 2.3 GeV in \sqrt{s} . (The 3D_2 partial wave from C500 is an exception, departing from the single-reaction analysis near threshold.) The upper limit to our single-energy analyses is due to a sharp cutoff in the number of data. This is apparent in Fig. 2 of Ref. [5]. Much additional data above 300 MeV will be required before a stable solution to 500 MeV can be expected.

A comparison of results for $\pi d \rightarrow pp$ reveals the most pronounced differences. One reason for this is the overall phase which was left undetermined in Ref. [7]. There, we arbitrarily chose the 3P_1S wave to be real. In the present analysis, the overall phase has been determined. In Fig. 4 we show that the 3P_1S phase is very different in the combined and separate analyses. Given the large difference in overall phase, we have chosen to compare the partial-wave amplitudes from the separate and combined analyses in terms of their moduli. This comparison is made in Fig. 5. As was the case for πd elastic scattering, differences are most significant above approximately 2.3 GeV in \sqrt{s} . A similar lack of data exists above this energy.

In general we see good agreement for the dominant amplitudes found in the separate and combined analyses. Figures 3 and 5 also display our single-energy analyses which

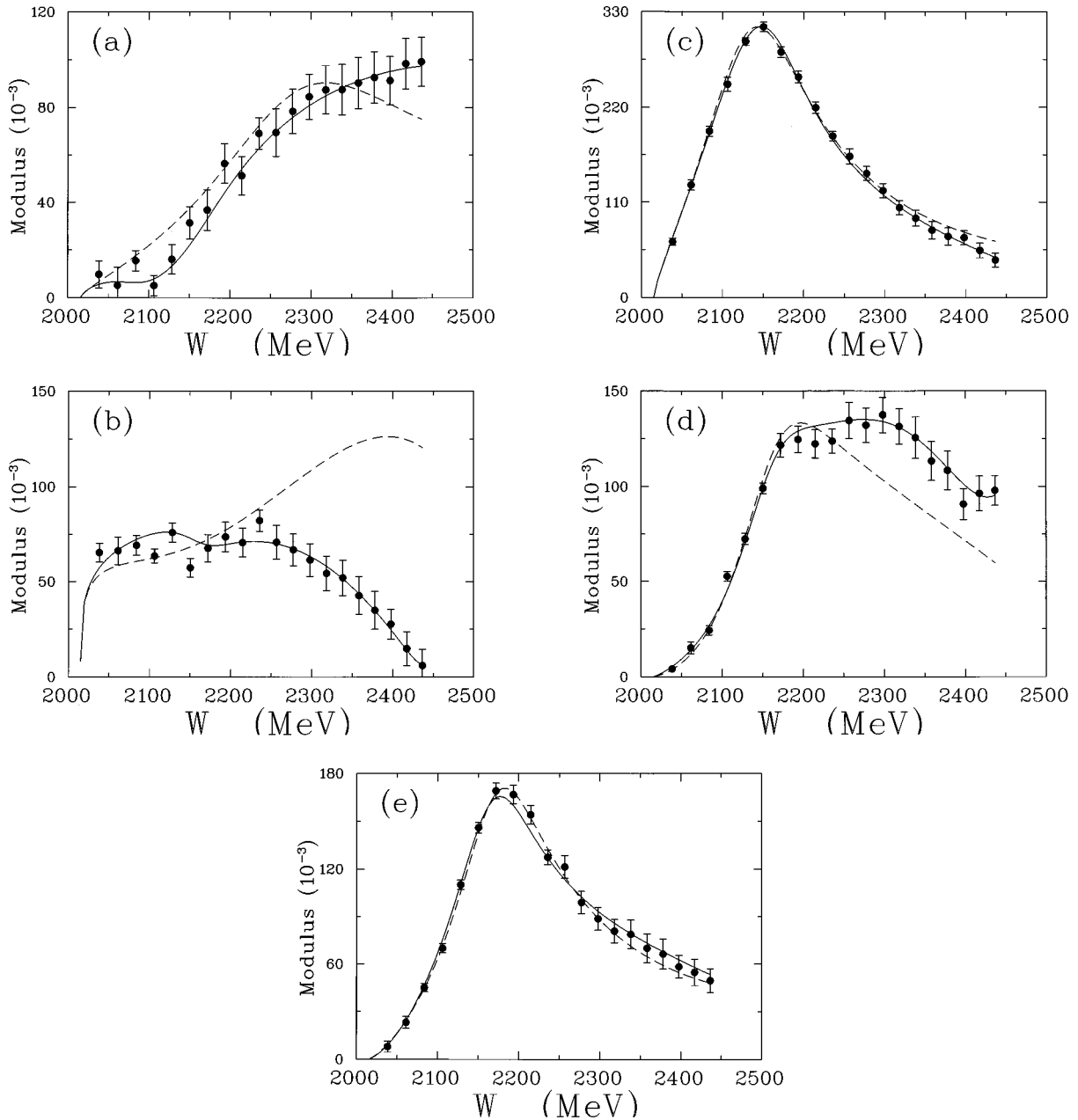


FIG. 5. Moduli of the partial-wave amplitudes for $\pi d \rightarrow pp$ from $T_\pi = 0$ to 500 MeV. The solid and dashed curves give the amplitudes corresponding to the C500 and SP96 [7] solutions, respectively. Moduli of the single-energy solutions are plotted as solid circles. All amplitudes have been multiplied by a factor of 10^3 and are dimensionless. Only dominant partial-waves have been plotted: (a) $^1S_0P(0^+)$, (b) $^3P_1S(1^-)$, (c) $^1D_2P(2^+)$, (d) $^3P_2D(2^-)$, and (e) $^3F_3D(3^-)$.

were done in order to search for structure which may be missing from the energy-dependent fit. (Details of the single-energy analyses are given in Refs. [5] and [7]. A comparison of the single-energy and energy-dependent fits is given in Tables III and IV.

IV. SUMMARY AND CONCLUSIONS

We have obtained new partial-wave amplitudes for πd elastic scattering and the reaction $\pi d \rightarrow pp$, using a K -matrix method which utilized information from our elastic pp scattering analysis. In addition to producing amplitudes more tightly constrained by unitarity, we have resolved the

overall phase ambiguity existing in our previous $\pi d \rightarrow pp$ analysis.

As mentioned in Sec. III, the combined analysis has resulted in a slightly improved fit to the πd elastic and $\pi d \rightarrow pp$ databases. The most noticeable differences, at the partial-wave level, appear at higher energies where the existing data are sparse. It is difficult to find cases where the fit has been dramatically improved. One exception is the set of πd total cross section data between 300 and 500 MeV. Here the combined analysis is much more successful in reproducing the energy dependence. The combined analysis gives total cross sections which begin to rise at 500 MeV, whereas the separate analysis shows a fairly monotonic decrease from

400 to 500 MeV. The behavior seen in the combined analysis seems reasonable, as the πd total cross sections do begin to rise just beyond the upper energy limit of our analysis. Many of the individual partial-wave amplitudes from C500 show rising imaginary parts near 500 MeV, a feature absent in the analysis of πd elastic data alone.

The present analysis has also resulted in a unified description of the resonancelike behavior previously noted in our separate analyses of pp [3] and πd [5] elastic scattering, and the reaction $\pi d \rightarrow pp$ [7]. This behavior [12] has been variously described as “resonant” (due to the creation of

dibaryon resonances) and “pseudoresonant” (due to the $N\Delta$ intermediate state). We expect that our combined analysis will further constrain models based on these two mechanisms.

ACKNOWLEDGMENTS

I.S. acknowledges the hospitality extended by the Physics Department of Virginia Tech. This work was supported in part by U.S. Department of Energy Grant No. DE-FG05-88ER40454.

-
- [1] H. Garcilazo and T. Mizutani, *πNN Systems* (World Scientific, Singapore, 1990).
- [2] F. Shimizu, Y. Kubota, H. Koiso, F. Sai, S. Sakamoto, and S. S. Yamamoto, Nucl. Phys. **A386**, 571 (1982); **A389**, 445 (1982).
- [3] R. A. Arndt, I. I. Strakovsky, and R. L. Workman, Phys. Rev. C **50**, 2731 (1994). We have used an updated version (WI96) of the published solution (SM94). Both solutions covered $T_p = 0$ –1600 MeV (for the np case we analyzed $T_n = 0$ –1300 MeV) or $\sqrt{s} = 1880$ –2560 MeV. For details, see [4].
- [4] These results and corresponding databases can be viewed and compared with previous analyses at the WWW site <http://clsaidd.phys.vt.edu> or through a Telnet call to vtinte.phys.vt.edu with user/password: physics/quantum, or to clsaidd.phys.vt.edu with user: said (no password).
- [5] R. A. Arndt, I. I. Strakovsky, and R. L. Workman, Phys. Rev. C **50**, 1796 (1994). We expect to have additional measurements of deuteron analyzing powers from PSI [6] in the near future.
- [6] G. Suft, Ph.D. thesis, Erlangen University, 1996; (private communication).
- [7] R. A. Arndt, I. I. Strakovsky, R. L. Workman, and D. V. Bugg, Phys. Rev. C **48**, 1926 (1993); **49**, 1229 (1994). We have used an updated version (SP96) of the published solution (SP93).
- [8] J. Nagata, M. Matsuda, N. Hiroshige, and T. Ueda, Phys. Rev. C **45**, 1432 (1992).
- [9] B. J. Edwards, Phys. Rev. D **23**, 1978 (1981); B. J. Edwards and G. H. Thomas, *ibid.* **22**, 2772 (1980).
- [10] The reader wishing to trace through the algebra leading to Eqs. (5) and (6) should see Chap. 17 of R. Levi Setti and T. Lasinski, *Strongly Interacting Particles* (University of Chicago Press, Chicago, 1973). This reference details the uses of full and reduced K matrices.
- [11] Relations between our amplitudes and observables for $\pi d \rightarrow pp$ and πd elastic scattering are given in Refs. [7] and [5], respectively. Relations between our pp helicity amplitudes and those used by other groups are given by R. A. Arndt, L. D. Roper, R. A. Bryan, R. B. Clark, B. J. VerWest, and P. Signell, Phys. Rev. D **28**, 97 (1983).
- [12] See, for example, I. I. Strakovsky, Fiz. Elem. Chastits At. Yadra **22**, 615 (1991) [Sov. J. Nucl. Phys. **22**, 296 (1991)], and references therein.